

# ES Materials and Manufacturing

DOI: https://dx.doi.org/10.30919/esmm1316



# Influence of Nanocrystalline Silicon Conductivity on the Structural and Optical Properties of Porous Silicon

Kadyrzhan Dikhanbayev, Isa Zharekeshev, Azamat Zhambyl, Yerulan Sagidolda,\* Zhansaya Baspakova, Bakyt Khaniyev, Nursultan Meirambekuly, Yeldos Kozhagulov and Shyryn Zhumatova\*

#### **Abstract**

Silicon substrates with p-n junction were layer-by-layer etched along the depth of the n-layer by the method of electrochemical anodization on the surface; the obtained porous silicon films were analyzed by means of voltammetric response, reflection spectra, and photoluminescence spectra as a function of the conductivity of the gradient layer along the depth of the p-n junction. It is shown that current flow across the thin-film layer, in particular, with the increase of the layer resistance along the etching depth, there appears a region of space charge associated with the depletion of charge in the vicinity of the p-n junction and an increase in the forward current-voltage characteristics, after which current rectification begins.

Keywords: Porous silicon films; Photon; Excited hole; Photoluminescence; Electrochemical etching; Nanostructures.

Received: 29 August 2024; Revised: 13 September 2024; Accepted: 03 October 2024.

Article type: Research article.

# 1. Introduction

In modern technologies, dielectric films play a crucial role in the field of micro-, nano, and optoelectronics, finding applications in light-emitting diodes (LEDs), photodetectors, vacuum microelectronics cathodes, biological implants, gas sensors, and membranes.<sup>[1,2]</sup> Among various dielectric films, silicon dioxide (SiO<sub>2</sub>) stands out as one of the most accessible and widely used materials, possessing significant potential for use in sensors and solar energy.<sup>[3]</sup>

In the synthesis of SiO<sub>2</sub>, methods such as magnetron sputtering, low-pressure chemical vapor deposition (LPCVD), thermal treatment of Si, and precipitation in a gel using tetra ethyl ortho silicate (TEOS) as a precursor material are often employed.<sup>[4]</sup> A particular advantage of the latter method is the formation of a continuous network of channels with a uniform distribution throughout the volume of silicon dioxide.

Special attention is given to ordered SiO<sub>2</sub> structures, as their properties differ from thin SiO films. Perpendicularly oriented arrays of SiO<sub>2</sub> cylinders are of particular interest due to densely packed frameworks, making them attractive for chemical reactions and optical applications. Control over the

Al-Farabi Kazakh National University, Al-Farabi ave. 71, Almaty, 050040, Kazakhstan.

\*Email: erulan.s@yandex.ru (Y. Sagidolda); shyryn.zhumatova@gmail.com (S. Zhumatova)

order of the structure can be achieved by altering the formation conditions and, consequently, the material's properties. Such ordered structures can be obtained using lithographic methods. In some published works, it is noted that porous silicon (PS) layers consist of pillars and Si pores or isolated nanocrystallites. On the other hand, PS can be considered a system of interconnected quantum wells, often referred to as a "quantum sponge".[5] However, it has been reported that the properties of PS, such as porosity, thickness, pore diameter, and the microstructure of silicon, depend on anodization conditions, including electrolyte, current density, plate type, resistivity, etching time, and temperature. [6,7] Study suggests that the origin of fluorescence can be explained by the presence of surface-bound molecular emitters, such as siloxanes. Another hypothesis asserts the existence of fluorescent surface particles trapped on the internal walls of the pores as a source of light emission.[8] Increasing the bandgap of PS is possible by reducing the size of nanocrystallites.[9] The mechanism of light emission in PS is not fully understood. One hypothesis suggests that luminescence occurs due to the quantum confinement of charge carriers in the narrow walls of crystalline silicon that pores. The initial report of visible photoluminescence (PL) at room temperature in PS structures sparked widespread interest in the scientific community regarding the derivative present in PS.[10] It has also been noted that the presence of small oxygen-related energy donors in the

range of 0.1 eV shows a clear correlation with the intensity of red PL observed in PS. A competing model for the source of luminescence is non-bridging oxygen hole centers. The study suggests that the source of PL in PS is a surface-bound emitter, as indicated by observed features resembling the PL of silicon-associated fluorophores linked to silicon oxyhydroxides. All hypotheses are based on the unique microstructure of PS with a large surface area characterized by high porosity and a crystalline structure with typical dimensions ranging from nanometers to several micrometers.

It is known that the conductivity of semiconductors increases under the influence of irradiation due to the absorption of photons in the semiconductor volume.[14] Promising in this direction is the use of silicon nanocrystals as the active sensing layer, as well as layers of wide-bandgap materials. In this case, the absorption spectrum of photoelectric converters expands into the short-wavelength range due to quantum size-induced widening of the forbidden band width in silicon nanocrystals and the absorption of highenergy photons in wide-bandgap materials. An effective system of silicon nanocrystals can be a layer of PS, as the walls of the pores form a disordered system of quantum wells, threads, and quantum dots. These processes involve the excitation of electrons from lower-lying free or bound states to higher free or bound states, as well as the recombination of excited electrons to their ground states.[15] Therefore, all semiconductors and some dielectrics based on semiconductors are materials whose conductivity changes under the influence of radiation.[16] The conductivity is also influenced by the carrier lifetime  $\tau$ , which is the time during which an excited electron remains in the conduction band  $(\tau_n)$  or an excited hole remains in the valence band  $(\tau_p)$ . The carrier lifetime is determined by the rate of surface and bulk recombination.

The carrier lifetime depends not only on the material properties but also on the surface condition, sample size, and manufacturing technology. In particular, chemical etching<sup>[17-19]</sup> of a polished sample surface allows for an increase in the carrier lifetime at the surface to the extent that the measured time, which corresponds to the surface recombination rate close to the bulk value, represents the carrier lifetime in the volume of the semiconductor.<sup>[20]</sup> Therefore, chemical texturing possesses passivating properties,<sup>[21]</sup> healing broken bonds within the structure.

Samples of nanocrystalline silicon obtained by chemical or electrochemical anodization<sup>[22-24]</sup> also exhibit conductivity when an external voltage is applied, although PS is closer to a dielectric semiconductor. This is because chemically etched surfaces of silicon undergo active surface oxidation of nanocrystallites.<sup>[25]</sup> Moreover, fluorescent properties of the Si/PS structure have been obtained,<sup>[26,27]</sup> including the infrared reflection spectrum, as well as the influence of etching current and solution composition on the sizes and shapes of SiO<sub>2</sub>.

Deep-etched nanocrystallites, with a resistance of over 2  $M\Omega$  silicon for both p- and n-type conductivity, have

photosensitivity in the forward and reverse branches of the current-voltage characteristic. [28,29] It is noticeable that the semiconductor conductivity  $\sigma$  after electrochemical etching of the surface of the diffusion layer sharply decreases with a change in the optical properties of PS. The research was conducted on pre-prepared diffusion p-n structures.

In this work, we will consider the gradient distribution of charge carriers, in which the electron concentration in the n+layer decreases towards the p-n junction. It is necessary to study the conductivity of nanocrystalline silicon under various surface etching conditions, and their effect on the PL spectra, reflection spectra, as well as on the structural and electrical properties of PS.

## 2. Experimental section

Monocrystalline p-type silicon with a resistivity of  $10~\Omega$ -cm and a thickness of  $350~\mu m$  was used as the starting material. Additionally, a pre-made structure with a p-n junction was utilized, where the n-layer was formed by phosphorus thermal diffusion at  $950~^{\circ}C$ , with a thickness of approximately 500-600~nm. For electrochemical anodization, a continuous ohmic contact made of Ni was formed on the back side using the chemical deposition method. Silicon substrates with p-n junctions were fractured into  $1~cm^2$  sample pieces and linear structures with an area of  $1.5\times0.2~cm^2$ . Subsequently, the samples were degreased in trichloroethylene, acetone, and isooctane through ultrasonic treatment, etched, thoroughly rinsed with deionized water, and dried.

The volt-ampere characteristics of the p-n structure were measured in the dark. The linear structure cross-sections are shown in Fig. 1. Point metal contacts based on an InGa alloy were applied to the surfaces of the linear PS structure. Silver wires were soldered to these contacts, and then volt-ampere characteristics were measured.

PS on the silicon surface was formed using the electrochemical anodization method in a solution of HF: ethanol in a 1:1 ratio in a specially designed polytetrafluoroethylene (PTFE) cell, with a current density ranging from 5 mA/cm² to 30 mA/cm² and etching times ranging from 3 seconds to 60 minutes. The prepared samples of PS were sent for the measurement of the electrical and optical properties of the nanostructures.

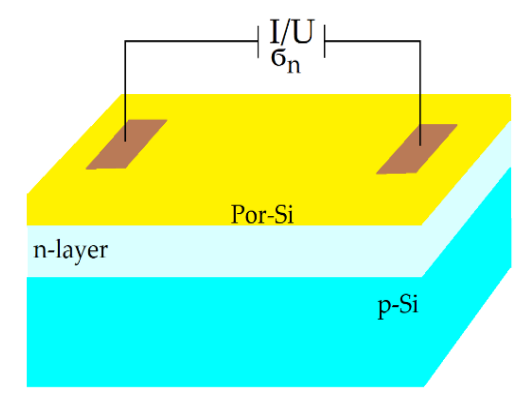


Fig. 1 The structure for measuring the volt-ampere characteristics.

ES Materials & Manufacturing Research article

The PL spectra were measured using the "Cary Eclipse Fluorescence Spectrophotometer" in the wavelength range from 300 nm to 1100 nm, with the excitation laser wavelength set at 488 nm.

A profile of the charge carrier concentration distribution was constructed through layer-by-layer etching of the surface of the n-layer down to the p-n junction. Additionally, the volumetric resistance *R* was measured across the depth of the p-n junction. Furthermore, current-voltage characteristics of the layer-by-layer etched gradient n-layer were recorded using a semiconductor analyzer.

The reflectance coefficients of PS samples were measured using the Lambda-35 setup in the spectral range from 300 nm to 1100 nm.

#### 3. Results and discussion

The directional change in concentration from the front surface is considered as a gradient concentration of electronic conductivity in the n-layer. To construct a profile of the electron concentration distribution across the depth of the p-n junction, the following electrical parameters will be determined after each electrochemical etching stage: conductivity, concentration, and etching depth. As known, the conductivity of charge carriers is determined by the formula. [30]

$$\sigma = ne\mu_n + pe\mu_p = e(n\mu_n + p\mu_p) \tag{1}$$

where e is the charge of an electron,  $\sigma$  is the conductivity, n is the electron concentration, p is the hole concentration, and  $\mu$  is the mobility. The initial surface concentration of the n-layer under thermal diffusion conditions was  $n_0 = 10^{19}$  cm<sup>-3</sup>. We determined the specific conductivity  $\sigma$  by measuring the resistivity of the porous layer using the 4-probe method after each electrochemical etching stage. The data are presented in Table 1.

**Table 1.** Results of resistivity measurements

$\rho$ , $\Omega$ ·cm	$\sigma$ ,( $\Omega$ ·cm) <sup>-1</sup>	<i>n</i> , cm <sup>-3</sup>	$X_{j}$ , $\mu$ m
$0.78 \times 10^{-3}$	1280	$8 \times 10^{18}$	0.05
$3.1 \times 10^{-3}$	320	$2 \times 10^{18}$	0.25
$1.56 \times 10^{-2}$	64	$4 \times 10^{17}$	0.4
$3.1 \times 10^3$	0.32×10 <sup>-3</sup>	$2 \times 10^{15}$	0.6

The depth of the p-n junction  $X_j$  was determined based on the conditions of phosphorus diffusion using the following relationship:<sup>[6]</sup>

$$X_j = 2\sqrt{D * \tau} \left(\ln \frac{N_D}{N_A}\right)^{\frac{1}{2}}$$
 (2)

where  $D=2\times 10^{-14}$  cm<sup>2</sup>/s is the phosphorus diffusion coefficient at a temperature of 950 °C,  $\tau=30$  minutes is the diffusion time,  $N_D$  is the electron concentration across the depth of the etched n-layer, and  $N_A\approx 2\times 10^{15}$  cm<sup>2</sup> is the initial hole concentration in the p-layer.

Figure 2 illustrates the distribution of charge carriers depending on the depth of the n-layer. It is evident that there is a sharp decrease in concentration as the thickness

approaches the p-n junction, leading to a reduction in electrical conductivity. Beyond the p-n junction, the concentration levels of the original silicon p-layer, *i.e.*, holes with  $N_A = 2 \times 10^{15}$  cm<sup>2</sup>, become apparent.

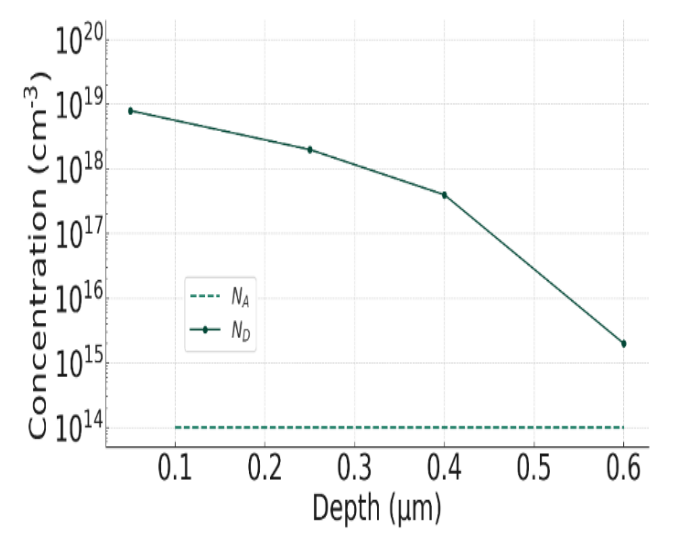
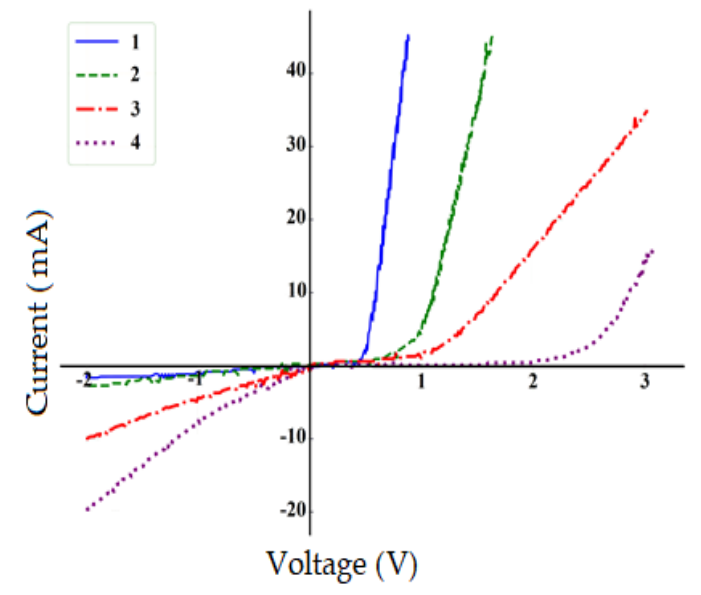


Fig. 2 shows the profile of electron concentration distribution after each etching of the n-layer surface, where  $N_D$  is the electron concentration, and  $N_A$  is the hole concentration.

The recorded current-voltage characteristics of the PS samples across the depth of the p-n junction are shown in Fig. 3. It is observed that the current-voltage characteristics undergo significant changes with increasing etching depth, particularly with the increase in the surface bulk resistance of the n-layer. For forward currents, as the voltage increases, the direct currents grow, and for reverse currents, leakage currents are also observed. Curve 1 corresponds to the current-voltage characteristics of the unetched original p-n junction, and it is evident that the current-voltage characteristics are close to an ideal shape.



**Fig. 3** The current-voltage characteristics of the depth-etched n-layer: 1-0 sec, 2-15 sec, 3-30 sec, 4-60 sec.

Curves 2 and 3 correspond to PS, anodized at a current density of 10 mA/cm² with etching times of 15 and 30 seconds, respectively. The series resistance gradually increases with the increase in leakage current. Curve 4 corresponds to an etching time of 60 seconds, where the forward current starts to rise only at around 2.0 V, and after that, rectification of the current begins.

The range from 0 to 2.0 V is the space-charge region, where the concentration of charge carriers is minimal. As is known, the sheet resistance is directly proportional to the cotangent of the slope angle, that is:

$$R_C = ctg\alpha = \frac{\Delta V}{\Delta I} \tag{3}$$

Therefore, from Fig. 3, it can be seen that as the tangent of the slope angle decreases, the resistance of the layer increases, thereby reducing the conductivity of the porous n-layer.

Reflection coefficients were measured across the depth of the n-layer in the spectral range from 400 nm to 1100 nm. The reflection of the original and etched PS samples is shown in Fig. 4. Reflection spectra of PS samples with short etching times in the short-wavelength range from 400 nm to 650 nm show minimal reflections ranging from 9% to 25%, respectively. Furthermore, in the visible range from 650-1100 nm, a slight increase in reflection from 20-37% is observed, due to the thinning of the film in the n-layer. Further reduction in the thickness of the n-layer leads to an optical thickness, indicating an increase in the transparency of the film.

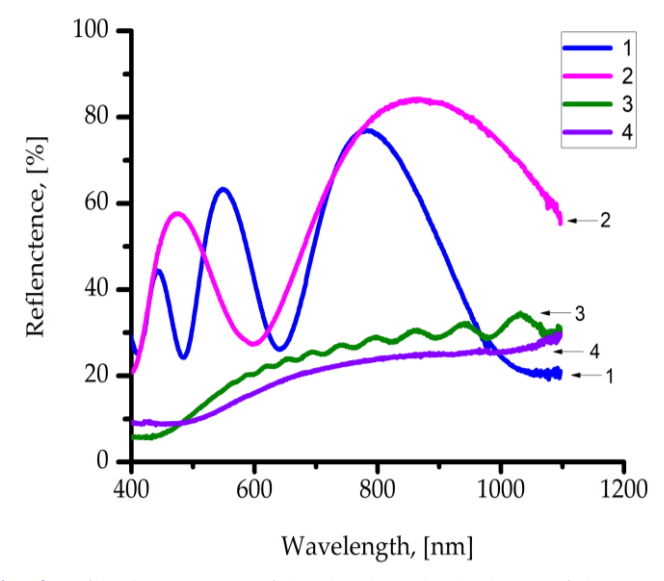


**Fig. 4** Reflection spectra of the depth-etched n-layer of the p-n junction: 1 - 0 sec, 2 - 15 sec, 3 - 30 sec, 4 - 60 sec.

As a result, the reflection spectrum of the film becomes an interference spectrum with a high refractive index, with reflections increasing on average in the short-wavelength range by 18% and in the long-wavelength range by up to 80%. The optical thickness is determined as:

$$d = \frac{\lambda}{4n(2m+1)} \tag{4}$$

where d is the optical thickness of the n-layer film, n is the refractive index of the film, and m is an integer (1, 2, 3,...).

Thus, with the decrease in the thickness of the n-layer, i.e., with the increase in the resistance of the spreading layer, the reflection coefficient sharply increases due to the reduction in the thickness of PS and the concentration of charge carriers.

As demonstrated earlier, porosity increases with longer etching times. It is known that the size of the silicon structure on the surface decreases with increasing anodization time. This leads to a shift of peaks towards lower wavelengths or higher energy with longer anodization times. This is consistent with the particle-in-a-box theory. The dependence of the energy gap on anodization time and PS layer thickness. Noticeable improvement in external quantum efficiency in the wavelength range from 700 to 1000 nm enhances light absorption at longer wavelengths, thus offering a promising opportunity to enhance light absorption in thin-film silicon solar cells. Additionally, electrochemical anodic oxidation at room temperature can be used as a surface passivation method for other nanostructured materials, as the thickness of the oxidized layer can be precisely controlled by adjusting the combination of current density and treatment period while preserving the original nanostructure.[31]

However, in our case, the PL spectra of the p-type PS sample and the etched PS sample with n-type conductivity were measured. Fig. 5 shows the intense PL spectrum of p-type conductive PS with a peak at a wavelength of 520 nm obtained under anodization conditions: 10 mA/cm<sup>2</sup> for 25 minutes.

The PL spectra of the gradient layer of PS were measured in the spectral range from 300 nm to 900 nm, along the depth of the porous n-layer. PL from each layer of the etched n-layer was measured separately to compare the intensity and shift of the fluorescence spectrum peaks. The PL of the selectively etched n-layer was measured separately to compare the intensity and shift of the fluorescence spectrum peaks.

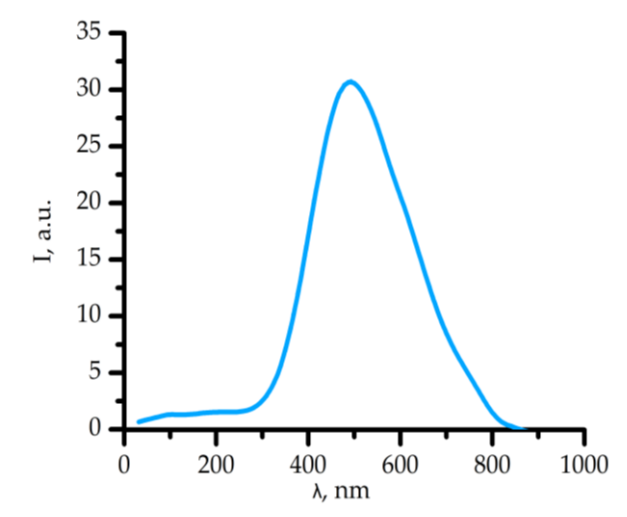


Fig. 5 The PL spectrum of PS for p-type conductivity.

For PS of n-type conductivity, the PL intensity is lower than that of p-type PS (Fig. 6). In the PL spectra (a), a sensitivity edge appears around 420 nm on the left, and after further etching for 5 seconds, a short-wavelength PL peak

ES Materials & Manufacturing Research article

while a peak around 420 nm is present. This shift in the peak suggests an enlargement of the bandgap of electrochemically The bandgap enlargement can be explained by the presence of nanowires and/or nanocrystalline phases in the deposited Si films.[32]

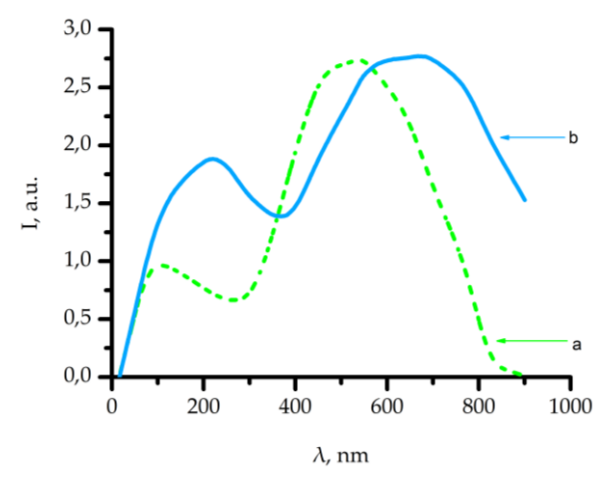


Fig. 6 The PL spectra of PS for n-type conductivity.

With further etching of the gradient n-layer for 10 seconds, the long-wavelength peak of PL disappears, and only the short-wavelength PL spectrum around 540 nm emerges (Fig. 7).

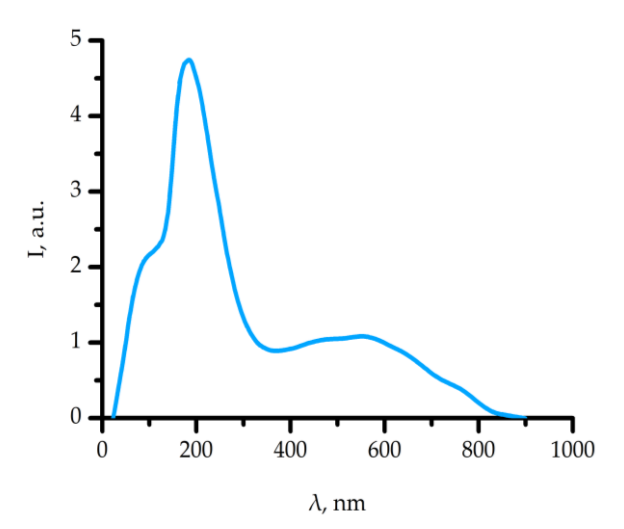


Fig. 7 PL spectrum of PS (10 s).

During subsequent etching of the gradient layer for 20 seconds, the PL spectrum of n-type PS completely diminishes (Fig. 8). In this case, we assume that the PS is finally etched out from the n-layer.

Therefore, etching the gradient n-layer depth-wise of the p-n junction leads to a change in the PL spectra, with a shift of the spectrum peak towards the short-wavelength side due to the quantum size effect.

Thus, the analysis of several experimental studies on gradient coatings depth-wise of the p-n junction indicates the reliability of measurements of electrical and optical

emerges. It can be seen that the peak at 620 nm decreases, characteristics. The repeatability and accuracy of the obtained results depend on the stability of creating nanocrystalline structures, the mode of producing nanoscience PS, and etched Si films compared to monocrystalline benchmark films. especially on the preparation of the HF: ethoxyethanol electrolyte composition.

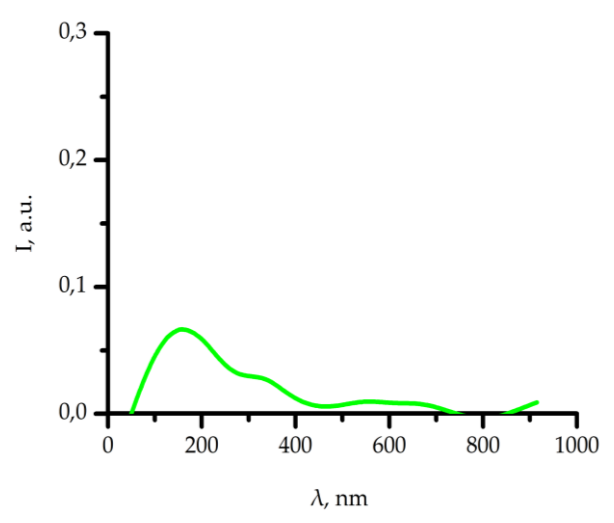


Fig. 8 PL spectrum of PS (20s).

The investigation of the etching depth concentration profile revealed a fascinating phenomenon of current passing through the thin film layer. Specifically, with the increase in the resistance of the layer with depth of etching, a space charge region arises associated with charge depletion near the p-n junction. This leads to an increase in the forward voltage, after which rectification of the current begins (Fig. 3).

The measurement of reflection spectra through the depth of the n-layer is also modified as it approaches the p-n junction boundary. In particular, the decrease in reflection occurs only in the short-wavelength region. After further etching, there is a sharp increase in the form of wave-like reflection, i.e., reflection spreads between the optical thickness in the immediate vicinity of the p-n junction (Fig. 4).

An interesting experimental analysis revealed the spectrum of PL through the depth of the p-n junction. The n-layer itself does not luminesce, and the nanostructures emit light when excited by short-wavelength radiation. This is because, in the process, both holes and electrons are generated. Etching proceeds through hole carriers, so we observe weak luminescence in the visible wavelength range (Fig. 6). As we approach the p-n junction, the reflections shift towards the short-wavelength side due to quantum confinement.

#### 4. Conclusions

A profile of the concentration distribution across the depth of the p-n junction was formed using successive chemical anodization of the n-layer surface. The specific conductivity, carrier concentration, and depth of the concentration distribution were determined.

From the voltamperometric characteristics, the nature of the changes in forward currents relative to the carrier concentration depth of the p-n junction was identified after each chemical etching. Additionally, the volt amperometric characteristics were used to determine the space-charge region where rectifying properties of the forward current occur with an increase in applied voltage.

The spectrum of light reflection with a change in conductivity in depth showed that there is a thickness of a high gas sensors, *Coating* concentration of carriers with a reflectance coefficient from 3%10.3390/coatings13010190. to 28% using this anodizing technology and also an optical thickness of the concentration with interference reflection of light ranging from 20 to 48% approaching the p-n transition. *Electronics*, 2003, 47, Changes in conductivity through depth significantly influence the spectra of PL in PS, causing a shift in the peak of the PL spectrum from the visible range at 520 nm to the short-wavelength range at 420 nm due to the quantum size effect.

## Acknowledgements

The research is funded under the project AP15473118 "Comprehensive Study of the Physical Characteristics of Silicon Nanostructures Obtained in a Solution Containing Hydrogen Hexafluorosilicate" and AP13268784 "Investigation of the Effect of Electrochemical Etching Modes on the Optical and Structural Properties of Porous Silicon" supported by the Committee of Science of the Ministry of Science and Higher Education of the Republic of Kazakhstan.

#### **Conflict of Interest**

There is no conflict of interest.

# **Supporting Information**

Not applicable.

# References

- [1] H. Wang, J. Zhang, J. Li, X. Lv, S. Zhang, G. Zhang, R. Sun, A strategy for the preparation of low dielectric FGQD/PSPI composite films in wafer-level packaging, *Materials Today Communications*, 2024, **40**, 110189, doi: 10.1016/j.mtcomm.2024.110189.
- [2] J. Mao, J. Chen, Z. Jia, T. Wang, H. Zhang, X. Lv, L. He, Q. Feng, W. Wang, F. Luo, Y. Qin, Z. Dang, Atom permeable gradient-structured hybrid dielectric films for highly improved capacitive energy storage, *Journal of Power Sources*, 2024, **619**, 235196, doi: 10.1016/j.jpowsour.2024.235196.
- [3] S. Thamri, M. H. Raouadi, Enhancement of NiO/Si solar cell by adding porous silicon and a silicon dioxide SiO<sub>2</sub> carrier selective layer, *Materials Letters*, 2024, **360**, 136002, doi: 10.1016/j.matlet.2024.136002.
- [4] N. Aboualigaledari, M. Rahmani, A review on the synthesis of the TiO<sub>2</sub>-based photocatalyst for the environmental purification, *Journal of Composites and Compounds*, 2021, **3**, 25-42, doi: 10.52547/jcc.3.1.4.
- [5] M. Das, P. Nath, D. Sarkar, Influence of etching current density on microstructural, optical and electrical properties of porous silicon (PS):n-Si heterostructure, *Superlattices and Microstructures*, 2016, **90**, 77-86, doi: 10.1016/j.spmi.2015.12.008.

- [6] V. Airaksinen, Handbook of Silicon Based MEMS Materials and Technologies, 2020.
- [7] B. Khaniyev, M. Ibraimov, Y. Sagidolda, Y. Tezekbay, T. Duisebayev, A. Tileu, A. Khaniyeva, The improved non-polar gas sensing performance of surface-modified porous silicon-based gas sensors, *Coatings*, 2023, 13, 190, doi: 610.3390/coatings13010190
- [8] T. Mizuno, Physical limitation of p-n junction—statistical variations of p-n junction depth in MOSFET array, *Solid-State Electronics*, 2003, 47, 957-962, doi: 10.1016/s0038-1101(02)00457-4.
- [9] E. L. Pankratov, Decreasing of depth of *p-n*-junction in a semiconductor heterostructure by serial radiation processing and microwave annealing, *Journal of Computational and Theoretical Nanoscience*, 2012, **9**, 41-49, doi: 10.1166/jctn.2012.1994.
- [10] J. Benick, K. Zimmermann, J. Spiegelman, M. Hermle, S. W. Glunz, Rear side passivation of PERC-type solar cells by wet oxides grown from purified steam, *Progress in Photovoltaics: Research and Applications*, 2011, **19**, 361-365, doi: 10.1002/pip.1020.
- [11] B. Ding, X. Huang, Z. Cai, Y. Ma, G. Song, W. Yang, C. Wen, Effects of binders on electrochemical properties of high-capacity silicon composite anodes, *Inorganic Chemistry Communications*, 2020, **113**, 107771, doi: 10.1016/j.inoche.2020.107771.
- [12] S. E. Guerrero, R. Nava, J. A. Reyes-Esqueda, Plasmonic-enhanced photoluminescence in porous silicon with pore-embedded gold nanoparticles fabricated by direct reduction of chloroauric acid, *Journal of Luminescence*, 2024, **269**, 120465, doi: 10.1016/j.jlumin.2024.120465.
- [13] W. Wu, M. Wang, R. Wang, Magnesio-mechanochemical reduced SiOx for high-performance lithium-ion batteries, *Journal of Power Sources*, 2018, **407**, 112-122, doi: 10.1016/j.jpowsour.2018.10.065.
- [14] B. K. Mohamid, U. M. Nayef, Z. F. Kadem, Chemical, morphological and electrical properties of porous silicon prepared by photelectrochemical etching, *Journal of Al-Nahrain University Science*, 2013, **16**, 145-115, doi: 10.22401/jnus.16.4.17.
- [15] Y. Hideyuki, N. Kunihiro, N. Shinji, I. Hideki, O. Shigeto, Investigation of the irreversible reaction mechanism and the reactive trigger on SiO anode material for lithium-ion battery, *Journal of the Ceramic Society of Japan*, 2011, **11**, 855-860, 10.2109/jcersj2.119.855.
- [16] M. Blanco-Loimil, A. Pardo, E. Villar-Alvarez, R. Martínez-González, A. Topete, S. Barbosa, P. Taboada, V. Mosquera, Development of ordered metal nanoparticle arrangements on solid supports by combining a green nanoparticle synthetic method and polymer templating for sensing applications, *RSC Advances*, 2016, **6**, 60502-60512, doi: 10.1039/c6ra04925g.
- [17] J. H. Shin, H. G. Kim, G. M. Baek, R. Kim, S. Jeon, J. H. Mun, H. -B. -R. Lee, Y. S. Jung, S. O. Kim, K. N. Kim, G. Y. Yeom, Fabrication of 50 nm scale Pt nanostructures by block copolymer (BCP) and its characteristics of surface-enhanced Raman scattering (SERS), *RSC Advances*, 2016, **6**, 70756-70762, doi: 10.1039/C6RA08608J.

ES Materials & Manufacturing Research article

[18] B. A. Khaniyev, Y. Sagidolda, K. K. Dikhanbayev, A. O. Tileu, M. K. Ibraimov, High sensitive NH<sub>3</sub> sensor based on electrochemically etched porous silicon, *Cogent Engineering*, 2020, **7**, 1810880, doi: 10.1080/23311916.2020.1810880.

- [19] S. A. Zhumatova, S. M. Manakov, Y. Sagidolda, M. B. Darmenkulova, R. M. Azamat, B. Y. Alpysbaeva, K. K. Dikhanbaev, Morphological, structural, and optical properties of silicon nanostructures formed in a solution containing hydrogen hexafluorosilicate H<sub>2</sub>(SiF6), *Optics and Spectroscopy*, 2020, **128**, 1487-1491, doi: 10.1134/s0030400x20090234.
- [20] M. B. Darmenkulova, M. B. Aitzhanov, S. A. Zhumatova, M. K. Ibraimov, Y. Sagidolda, Change of optical properties of carbon-doped silicon nanostructures under the influence of a pulsed electron beam, *Journal of Nanotechnology*, 2022, 2022, 1320164, doi: 10.1155/2022/1320164.
- [21] B. Roman-Manso, E. Domingues, F. M. Figueiredo, M. Belmonte, P. Miranzo, Enhanced electrical conductivity of silicon carbide ceramics by addition of graphene nanoplatelets, *Journal of the European Ceramic Society*, 2015, **35**, 2723-2731, 10.1016/j.jeurceramsoc.2015.03.044.
- [22] B. Roman-Manso, F. M. Figueiredo, B. Achiaga, R. Barea, D. Perez-Coll, A. MorelosGomez, M. Terrones, M. I. Osendi, M. Belmonte, P. Miranzo, Electrically functional 3D-architectured graphene/SiC composites, *Carbon*, 2016, **100**, 318-328, doi: 10.1016/j.carbon.2015.12.103.
- [23] K. Markandan, J. K. Chin, M. T. T. Tan, Recent progress in graphene based ceramic composites: a review, *Journal of Materials Research*, 2017, **32**, 84-106, doi: 10.1557/jmr.2016.390.
- [24] O. Hanzel, Z. Lences, Y. W. Kim, J. Fedor, P. Saigalik, Highly electrically and thermally conductive silicon carbidegraphene composites with yttria and scandia additives, *Journal of the European Ceramic Society*, 2020, **40**, 241-250, 10.1016/j. jeurceramsoc.2019.10.001.
- [25] Y. Taki, M. Kitiwan, H. Katsui, T. Goto, Electrical and thermal properties of off-stoichiometric SiC prepared by spark plasma sintering, *Journal of Asian Ceramic Societies*, 2018, **6**, 95-101, doi: 10.1080/21870764.2018.1446490.
- [26] R. Malik, Y. W. Kim, I. H. Song, High interfacial thermal resistance induced low thermal conductivity in porous SiC-SiO<sub>2</sub> composites with hierarchical porosity, *Journal of the European Ceramic Society*, 2020, **40**, 594-602, doi: 10.1016/j.jeurceramsoc. 2019.10.056.
- [27] D. Martín-Sánchez, T. Angelova, J. García-Rupérez, Simultaneous refractive index sensing using an array of suspended porous silicon membranes, *IEEE Sensors Journal*, 2020, **20**, 8497-8504, doi: 10.1109/JSEN.2020.2983218.
- [28] S.-W. Seo, H. R. Azmand, A. N. Enemuo, Hollow core waveguide sensor array based on a macroporous silicon membrane structure, *Journal of Lightwave Technology*, 2019, **37**, 2036-2041, doi: 10.1109/JLT.2019.2897427.
- [29] E. Luais, F. Ghamouss, J. Sakai, T. Defforge, G. Gautier, F. Tran-Van, Improved cycling performances of binder-free macroporous silicon Li-ion negative electrodes using room

temperature ionic liquid electrolyte, *Journal of Solid State Electrochemistry*, 2019, **23**, 937-941, doi: 10.1007/s10008-019-04197-6.

- [30] J. P. Colinge, C. A. Colinge, Physics of Semiconductor Devices Springer Science & Business Media, 2005.
- [31] P. Sundarapura, X.-M. Zhang, R. Yogai, K. Murakami, A. Fave, M. Ihara, Nanostructure of porous Si and anodic SiO<sub>2</sub> surface passivation for improved efficiency porous Si solar cells, *Nanomaterials*, 2021, **11**, 459, doi: 10.3390/nano11020459.
- [32] G. Ledoux, J. Gong, F. Huisken, O. Guillois, C. Reynaud, Photoluminescence of size-separated silicon nanocrystals: confirmation of quantum confinement, *Applied Physics Letters*, 2002, **80**, 4834-4836, doi: 10.1063/1.1485302.

**Publisher's Note:** Engineered Science Publisher remains neutral with regard to jurisdictional claims in published maps and institutional affiliations.